A Validated Solution for the Threat of Ionosphere Spatial Anomalies to Ground Based Augmentation System Users

*Sam Pullen[1], Jiyun Lee[2], Seebany Datta-Barua[3], Young Shin Park[4], Godwin Zhang[5], and Per Enge[6]

[1]Aeronautics and Astronautics, Stanford Univ. (E-mail: spullen@stanford.edu)
[2]Aeronautics and Astronautics, Stanford Univ. (E-mail: jjlee@relgyro.stanford.edu)
[3]Aeronautics and Astronautics, Stanford Univ. (E-mail: seebany@stanford.edu)
[4]Aeronautics and Astronautics, Stanford Univ. (E-mail: yspark@stanford.edu)
[5]Aeronautics and Astronautics, Stanford Univ. (E-mail: godwin@stanford.edu)
[6]Aeronautics and Astronautics, Stanford Univ. (E-mail: per.enge@stanford.edu)

Abstract

This paper develops a complete methodology for the mitigation of ionosphere spatial anomalies by GBAS systems fielded in the Conterminous U.S. (CONUS). It defines an ionosphere anomaly *threat model* based on validated observations of unusual ionosphere events in CONUS impacting GBAS sites in the form of a linear "wave front" of constant slope and velocity. It then develops a simulation-based methodology for selecting the worst-case ionosphere wave front impact impacting two satellites simultaneously for a given GBAS site and satellite geometry, taking into account the mitigating effects of code-carrier divergence monitoring within the GBAS ground station. The resulting maximum ionosphere error in vertical position (MIEV) is calculated and compared to a unique vertical alert limit, or $VAL_{H2,I}$, that applies to the special situation of worst-case ionosphere gradients. If MIEV exceeds $VAL_{H2,I}$ for one or more otherwise-usable subset geometries (i.e., geometries for which the "nominal" vertical protection level, or VPL_{H0}, is less than the "normal" VAL), the broadcast σ_{pr_gnd} and/or σ_{vig} must be increased such that all such potentially-threatening geometries have $VPL_{H0} > VAL$ and thus become unavailable. In addition to surveying all aspects of the methods used to generate the required σ_{pr_gnd} and σ_{vig} inflation factors for CONUS GBAS sites, related methods for deriving similar results for GBAS sites outside CONUS are suggested.

Keywords: GBAS, Integrity, Ionosphere, Threat Model, Protection Level, Alert Limit

1. Introduction

The potential threat of ionosphere spatial gradient anomalies to ground based augmentation systems (GBAS) was discovered in 2002 during analyses of WAAS ionosphere data for the 6 – 7 April 2000 ionosphere storm in the Conterminous U.S. (CONUS) [2]. Spatial ionosphere gradients during that storm were many times the 2 – 4 mm/km (zenith, 1σ) that are typical during nominal conditions, even during active ionosphere periods [5]. While the threat to GBAS from that storm was being studied, more-severe ionosphere storms occurred in late October and November 2003 following a major solar Coronal Mass Ejection [3,4].

This paper presents an overview of the multi-step method developed since 2003 to address the threat posed by ionosphere storms in CONUS. Section 2 discusses the development of a linear wave front ionosphere anomaly "threat model" with "worst-case" bounds on ionosphere gradient slope, speed, and width. Section 3 explains how this threat model is utilized in simulations that determine the largest ionosphere-induced range and position errors that are not detected (with the required missed-detection probability) by ground-system code-carrier divergence (CCD) monitoring. It also shows how the results of these simulations are used to generate σ_{pr_gnd} and σ_{vig} inflation factors in real-time (adjusting for the current satellite geometry) or by setting fixed, worst-case inflation factors offline and infrequently updating them. This latter approach simplifies the GBAS ground station design at the cost of reduced availability and additional maintenance requirements.

While a significant amount of ionosphere-anomaly data exists for CONUS, the same does not appear to be true for other regions of the world where GBAS will be fielded. Section 4 discusses variations of the ionosphere methodology used for CONUS that could be used in these regions. If these methods are based on less data than is available for CONUS, additional conservatism may be needed, particularly in areas near the Geomagnetic equator. Section 5 briefly summarizes this paper.

2. CONUS Ionosphere Anomaly Threat Model

2.1 CONUS Ionosphere Anomaly Database

Table 1 gives a list of days which were determined by the study of post-processed WAAS "supertruth" data [7] to have potentially hazardous ionosphere gradients for GBAS. These days were analyzed using the method described in [3]. Of the days shown in Table 1, only the highlighted rows covering four days (29 – 31 October 2003 and 20 November 2003) had gradients severe enough to be hazardous to GBAS users performing CAT I precision approaches, and of these, 20 November 2003 was the most severe day [1,3,4]. Figure 1 shows what happened on this day – it shows a plot of ionosphere delay vs. time in the afternoon local time (early evening UT) at a cluster of 7 nearby CORS stations in Northern Ohio and Southern Michigan. The onset of a "bubble" of very high ionosphere delays, with sharp gradients in time and space on both sides of the bubble (and, to a lesser degree, inside the bubble), is evident. Further analysis suggested that the bubble of enhanced ionosphere delay generating these measurements was oriented roughly from Northwest to Southeast and was

Table 1. CONUS Ionosphere Storm Days Analyzed

Day (UT)	K_P	D_{ST}	Geo. Storm Class	WAAS Coverage	Focus Region
4/6/2000	8.3	– 287	Severe	None (pre-IOC)	NE Corridor
4/7/2000	8.7	– 288	Extreme	None (pre-IOC)	NE Corridor
7/15/2000	9.0	– 289	Extreme	None (pre-IOC)	N/A
7/16/2000	7.7	– 301	Strong	None (pre-IOC)	N/A
9/7/2002	7.3	–163	Strong	None (pre-IOC)	N/A
10/29/2003	9.0	– 345	Extreme	~ 0%	N/A
10/30/2003	9.0	– 401	Extreme	~ 0%	TX-OK-LA-AR
10/31/2003	8.3	– 320	Severe	~ 0%	FL-GA
11/20/2003	8.7	– 472	Extreme	~ 0%	OH-MI
7/17/2004	6.0	– 80	Moderate	~ 68.8%	TX-OK-LA-AR

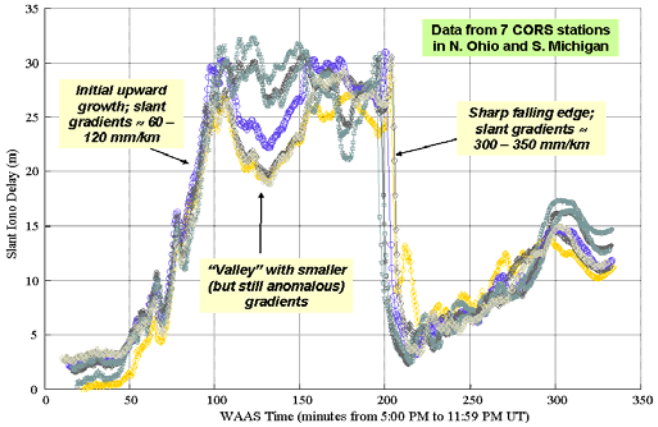

Figure 1. Severe Ionosphere Gradients in Ohio/Michigan Region during 20 November 2003 Ionosphere Storm

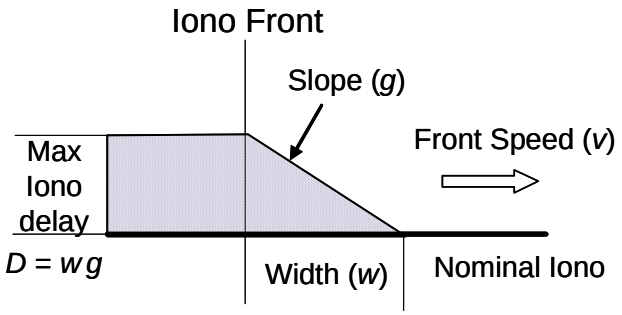

Figure 2. Linear Wave-Front Model of Ionosphere Anomaly

moving roughly West-South-Westward at approximately 200 m/s relative to the ground [3]. Based on similar findings from the other storms in Table 1, a simplified physical model of a linear ionosphere gradient wave front affecting a GBAS ground station and user was created and is described in Section 2.2.

2.2 CONUS Ionosphere Anomaly Threat Model

Figure 2 illustrates the constant, linear gradient "wave front" model of an ionosphere spatial gradient used in the ionosphere anomaly threat model developed as part of this research [1,3]. The three key parameters of this model are wave front width (w) in km, wave front propagation speed (v) with respect to a fixed point on the ground in m/s, and the gradient or slope of the change of slant ionosphere delay (g) in mm/km. Note that the total change in ionosphere delay (D) is given by:

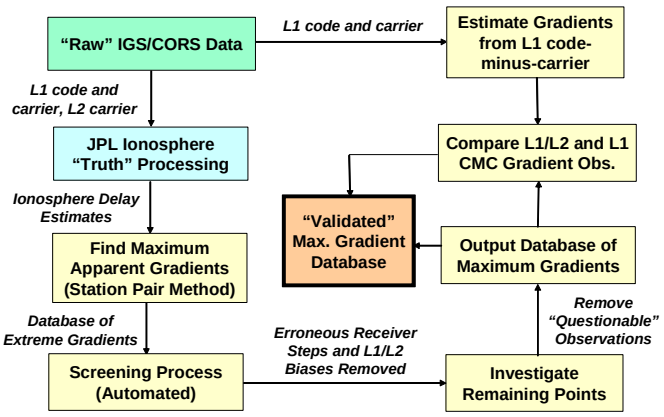

Figure 3. Ionosphere Anomaly Data-Analysis Procedure

$$D = w\,g\,. \qquad (1)$$

Data analysis based on the process detailed in [3] is used to establish limits on each of these four parameters to serve as bounds for the ionosphere anomaly threat model. Figure 3 summarizes this process and identifies two parallel tracks of data processing. In one, dual-frequency (L1/L2) data post-processed by Attila Komjathy of the Jet Propulsion Laboratory (JPL) in Pasadena, California (see [7]), is searched to find the maximum apparent ionosphere gradients that survive an automated screening process intended to remove erroneous receiver measurements that might appear to be large ionosphere gradients. In the other, raw L1-only data is downloaded directly from the CORS Internet website [9] and is used to estimate ionosphere gradients from L1 code-minus-carrier (CMC) calculations.

Once gradient estimates from both L1/L2 and L1 CMC are available, manual investigation by teams of experts and graduate students at Stanford University was used to sort out actual gradients from the much larger population of "false gradients" created by receiver errors not detected by automated screening, loss of lock on L2 and (much less frequently) L1 signals due to low C/N_0 and/or ionosphere scintillation, and incorrect L1/L2 receiver bias estimates. The remaining events for satellites above 12° elevation that could be verified with sufficient confidence to be actual ionosphere spatial gradients are shown in Figure 4 as functions of estimated slant gradient (g) and speed (v) [1]. The third parameter, width (w), is not shown because it is difficult to estimate independently from speed and, given that the width in all cases appears to be at least 25 km, the exact width is not critical to the impact on LAAS users.

Given the results in Figure 4, values representing the extreme (worst-case) bounds on the parameters g, v, w, and D were selected by drawing line segments to include the points included in Figure 4 (and similar plots for satellites below 12° elevation) plus the outer ends of the measurement error bars shown in Figure 4. The resulting outer bounds are loosely expressed in Table 2 (on the following page) and are more precisely expressed by the following set of nine equations [1]:

$$V_{front} \le 90\ m/s\,,\quad Slope_{vel}(V_{front}) = 125\ \ mm/km \qquad (2)$$

$$90 < V_{front} \le 108\,,\quad Slope_{vel}(V_{front}) = \frac{(177-125)}{(108-90)}(V_{front} - 90) + 125\ \ mm/km \qquad (3)$$

$$108 < V_{front} \le 115\,,\quad Slope_{vel}(V_{front}) = \frac{(211-177)}{(115-108)}(V_{front} - 108) + 177\ \ mm/km \qquad (4)$$

$$115 < V_{front} \le 158\,,\quad Slope_{vel}(V_{front}) = \frac{(258-211)}{(158-115)}(V_{front} - 115) + 211\ \ mm/km \qquad (5)$$

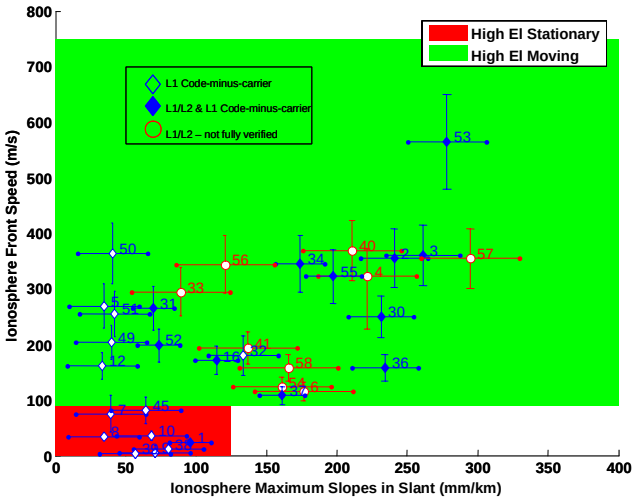

Figure 4. Verified Ionosphere Anomalies for Satellites above 12 Degrees Elevation

$$158 < V_{front} \le 354\ ,\ \ Slope_{vel}(V_{front}) = \frac{(330-258)}{(354-158)}(V_{front} - 158) + 258\ \ mm/km \quad (6)$$

$$V_{front} > 354\ \ m/s\ ,\ \ \ Slope_{vel}(V_{front}) = 330\ mm/km \quad (7)$$

$$El \le 35°\ ,\ \ Slope_{el}(El) = \frac{(330-50)}{35}(El) + 50\ \ mm/km \quad (8)$$

$$El > 35°\ ,\ \ Slope_{el}(El) = 330\ \ mm/km \quad (9)$$

$$Slope(V_{front}, El) = Min(Slope_{el}(El), Slope_{vel}(V_{front})) \quad (10)$$

Here, El denotes the satellite elevation angle in degrees and V_{front} denotes the ionosphere wave front propagation speed in m/s. Equations (2 – 7) define the maximum slope as a function of front speed for six distinct ranges of V_{front}, while (8, 9) define this slope as a function of elevation angle below and above 35°. Equation (10) establishes the final slope bound as the lower of the bound based on V_{front} (or $Slope_{vel}$) from equations (2 – 7) and the bound based on elevation angle (or $Slope_{el}$) from (8, 9).

Table 2 summarizes the bounding slope, speed, width, and maximum ionosphere delay difference values without respect to speed or elevation via equations (2 – 10). It shows bounds not obvious from (2 – 10), including a slope constraint of 150 mm/km for elevations below 12° and a slope constraint of 125 mm/km for front speeds below 90 m/s [4]. Also note that while the maximum slope based on front speed saturates at 354 m/s as per (7), the actual maximum speed is 750 m/s (although the fastest speed confidently observed is below 700 m/s, as shown in Figure 4). Finally, it should be noted that the maximum delay

Table 2. CONUS Threat Model Outer Bounds

Elevation	Speed	Width	Slope (slant)	Delay Diff.
Low elevation (< 12°)	90 – 750 m/s	25 – 200 km	30 – 150 mm/km	30 m
	0 – 90 m/s	25 – 200 km	30 – 125 mm/km	25 m
High elevation (= 12°)	90 – 750 m/s	25 – 200 km	30 – 330 mm/km(†)	50 m(*)
	0 – 90 m/s	25 – 200 km	30 – 125 mm/km	25 m

(*) Max. error constrains possible slope/width combinations
(†) Max. gradient is a function of speed and elevation angle

difference does not constrain the threat model except for the case of fast-moving wave fronts affecting satellites above 12°, where it is possible for a combination of allowed slope and width to exceed the allowed maximum delay of 50 m. For example, if g = 300 mm/km and w = 175 km, applying equation (1) gives $D = w\,g$ = 52.5 m, which exceeds the 50-meter maximum constraint on D. In this case, the fact that given choice of (w, g) exceeds this constraint means that the selected (w, g) pair is not in the threat model, even though the individual values of w and g are inside the allowed width and slope bounds.

Section 3 to follow describes how our simulation of ionosphere anomaly effects on GBAS makes use of this threat model. The starting point for this analysis is the determination of the anomaly parameters within the threat model that maximize the resulting user differential range error for a given satellite or combination of satellites in view of the GBAS ground station. Because each satellite has its own elevation angle and (theoretical) ionosphere pierce point (IPP) velocity (see [1,2]), this "worst-case" point within the threat model will vary with each satellite or combination of satellites in view. However, what is of interest for any given satellite geometry is the worst-case point within the threat model rather than an ensemble or average risk posed by all of the threat model points put together.

3. Simulation of Worst-Case GBAS User Errors

Figure 5 lays out the five procedures included in the GBAS ionosphere anomaly impact simulation developed for CONUS, which is described in more detail in [1]. The first element, the threat model, has already been detailed in Section 2. The remaining elements are described in Sections 3.1 (the 2nd and 3rd elements), 3.2 (the 4th element), and Section 4 (the 5th element).

3.1 Maximum Range Error Determination

The second element of Figure 5 is a simulation of the maximum ionosphere-induced range error (MIER) on an individual satellite in view of the GBAS ground station. As noted above, the worst-case combination of parameters within the ionosphere anomaly threat model for a given satellite depends on that satellite's elevation angle and theoretical ionosphere pierce point speed (V_{IPP}) as given by the traditional ionosphere shell model, which concentrates all ionosphere delay at a "shell height" which for GPS is normally taken to be 350 km. The key parameter in determining the worst-case anomaly is [1]

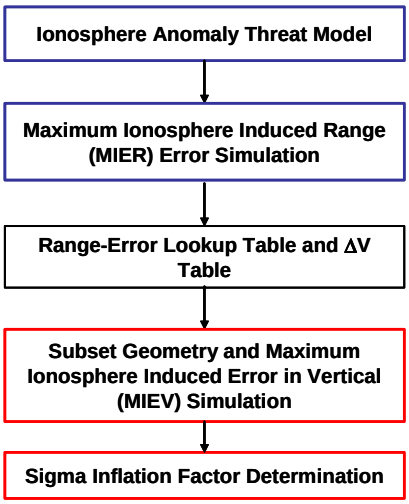

Figure 5. Elements of GBAS Ionosphere Anomaly Simulation

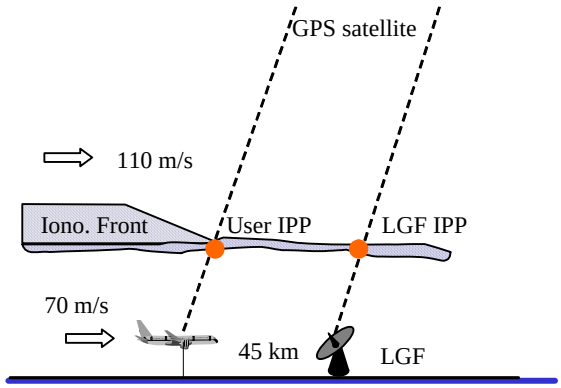

Figure 6. Potentially-Threatening Aircraft Approach Direction

$$dV_{front|IPP} = V_{front} - V_{IPP} . \quad (11)$$

Here, V_{front} is the same as v from the threat model description in Section 2 – it is the velocity of the ionosphere wave front relative to a fixed point on the ground, such as the GBAS ground station. Subtracting off V_{IPP} (and noting that this is a 2-D vector subtraction) as shown in (11) results in the wave front velocity as seen by the GBAS ground station. The FAA implementation of this ground station is known as the LAAS Ground Facility (LGF) and includes code-carrier divergence (CCD) monitoring to detect anomalous ionosphere variations in time soon after they become visible to the LGF. The CCD monitor inside the LGF (see [1,11] for details) has a divergence detection threshold of about 0.023 m/s and is almost guaranteed to exclude satellites with an observed ramp divergence of 0.04 m/s or greater within 100 seconds of onset. Note that divergence caused by the ionosphere is equivalent to twice the ionosphere rate-of-change, so the divergence numbers reported above would be halved when representing ionosphere rate-of-change, or "I-dot".

As shown in Figure 6, because effective monitoring exists within the LGF, the set of wave front approach directions that threatens user aircraft performing precision approaches is limited to the subset that impacts the airplane before reaching the LGF. In Figure 6, the approaching aircraft, which does not have its own monitor, is impacted by the moving gradient for some time before the gradient reaches the LGF. This would be the case if V_{IPP} were near zero (i.e., the satellite's elevation were near 90°). The situation could be worse if V_{IPP} were near 110 m/s (the magnitude of V_{front}) and in the same direction as V_{front}). In that case, no threat would exist if the "start" of the front were as shown in Figure 6 because the front would never "catch up to" the IPP of the aircraft shown before it lands. If, instead, the front were located just to the left of the LGF IPP, it would have already affected the aircraft while never becoming visible to the LGF, leading to a potentially serious (and undetected) range error.

The key point to understand is that the observance of a ramp divergence or I-dot within the LGF is dependent on the translation of spatial gradient into temporal gradient, and this requires a non-zero value of $dV_{front|IPP}$ (which, for simplicity, is also denoted as ΔV). Therefore, the simulation carried out in the second element shown in Figure 5 determines the maximum ionosphere-induced differential range error as a function of both gradient and speed (maximizing over all widths) where speed is interpreted as $dV_{front|IPP}$; i.e., speed relative to the IPP. The third element shown in Figure 5 is a data-interface function that transforms the tables provided by the range-domain simulation (performed by Mats Brenner of Honeywell) into the format needed by the position-domain simulation run at Stanford that is described in the following section.

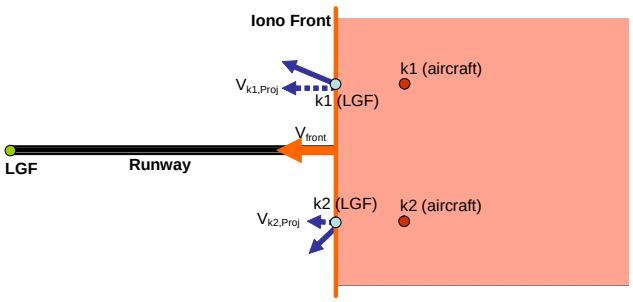

Figure 7. Model of Worst-Case Front Impact on Satellite Pair

3.2 MIEV and Sigma Inflation Factor Determination

The fourth element in Figure 5 (described in detail in [1]) adds a specific LGF location and generates all-in-view and subset GPS satellite geometries (down to all subsets of four satellites) for that location over a repeatable 24-hour day. In addition, for each of these geometries, it simulates all possible impacts of anomalous ionosphere wave fronts on all independent pairs of IPPs within that geometry (i.e., simultaneous impacts on two different IPPs). The decision to represent the worst-case dual-satellite impact as possible for CAT I operations appears extremely conservative to the primary author of this paper given that the worst possible point within the threat model is chosen to represent the anomaly scenario with a probability of 1.

In reality, it is practically impossible to find the absolute worst dual-satellite ionosphere scenario given that, while the threat model geometry in Figure 2 is linear, the data listed in Table 1 does show curves and back-and-forth bends over latitude and longitude. However, given complete flexibility to bend, the worst-case front would be impossible to defend against. The geometry used in the Stanford simulation is shown in Figure 7 and represents a compromise between these two extremes [1]. In Figure 7, the two satellites being impacted are designated k_1 and k_2. Two separate ionosphere wave fronts are constructed for this pair. The first such front is one that is "optimized" to give the maximum possible range error for satellite k_1. The resulting wave-front parameters are then propagated (assuming a straight-line front) to satellite k_2 and the resulting range error on k_2 is derived via table look-up based on these parameters. If the resulting error on k_2 does not have the same sign as the error on k_1 (meaning that the contribution of k_2 would detract from the total error of the k_1/k_2 pair), the error contribution of k_2 is set to zero instead, which insures that this dual-satellite-impact approach is never better than a single-satellite impact on k_1. The second front generated for this pair is simply the reverse case of the first front. In this second case, the front parameters are selected to maximize the error on satellite k_2, then these front parameters are propagated to satellite k_1, and k_1's contribution is either added to that of k_2 (if it adds more error) or is set to zero (if it would subtract error). Finally, the maximum range error selected for this pair of satellites is the greater error (in absolute value) of the two wave-front cases generated by this method.

Given the worst-case ionosphere-induced range error for each pair, the maximum ionosphere error in vertical (position), or MIEV, for that pair can be calculated as follows [1]:

$$MIEV_{k1,k2} = \left| S_{vert,k1}\varepsilon_{I,k1} + S_{vert,k2}\varepsilon_{I,k2} \right| + K_{MD}\sqrt{\sum_{i=1}^{N_c} S_{vert,i}^2 \sigma_i^2} \quad .(12)$$

Here, K_{MD} represents the "missed-detection buffer" of additional nominal vertical position error that must be allowed for to

achieve a given risk allocation (a small fraction of the 2×10^{-7} per approach total signal-in-space integrity requirement from [10]) presuming a (very conservative for CONUS) prior probability of the worst-case ionosphere anomaly of 10^{-5} per approach, which is the same probability assumed for other anomalies (see [6]). $S_{vert,i}$ is vertical-position-axis entry for satellite i (from 1 to N_C usable satellites in this subset geometry) in the range-to-position solution matrix $\boldsymbol{S}$ defined in Section 2.3.9 of [6], and σ_i^2 is the nominal error variance for satellite i as defined in Section 2.3.9 of [6]. The corresponding MIEV equation for the case where the threat is limited to the worst single-satellite impact is similar and can be derived by a subset of the method described above:

$$MIEV_k = \left| S_{vert,k} \varepsilon_{I,k} \right| + K_{MD} \sqrt{\sum_{i=1}^{N_C} S_{vert,i}^2 \sigma_i^2} \ . \qquad (13)$$

In order for a given set of visible GPS satellites (minus those flagged as unhealthy or otherwise excluded by the GBAS ground station) to be acceptable from the point-of-view of potential ionosphere anomalies, every usable subset of these satellites must be "safe". A "usable" satellite subset is defined as one with four or more satellites (to allow for a position solution) and with $VPL_{H0} \le VAL$ along the entire approach. In this case, "VAL" is the standard Vertical Alert limit for Category I precision approaches defined in Section 3.2.5.9.3 of [10] and Section 2.3.11.5.2.1.1.2 of [6], and VPL_{H0} for Category I precision approach is defined as follows (see [6], where K_{ffmd} depends on the number of reference receivers and is about 5.8):

$$VPL_{H0} = K_{ffmd} \sqrt{\sum_{i=1}^{N_C} S_{vert,i}^2 \sigma_i^2} \ . \qquad (14)$$

Geometries which meet the $VPL_{H0} \le VAL$ constraint must pass another test to meet the integrity requirement [1]:

$$\max \{MIEV_{k1,k2}\} \le VAL_{H2,I} \ . \qquad (15)$$

Here, $VAL_{H2,I}$ is an entirely new vertical alert limit that is not known by GBAS users and only applies to the analysis of potential ionosphere anomalies. Two separate and unrelated justifications for it exist. One is the excess conservatism applied to the analysis of worst-case ionosphere anomalies as described above, and the other is the growing confidence within the FAA that precision approaches to a 200-ft decision height can be supported with effective FASVAL's (VAL's at the decision height) of as large as 35 meters. Validation of these

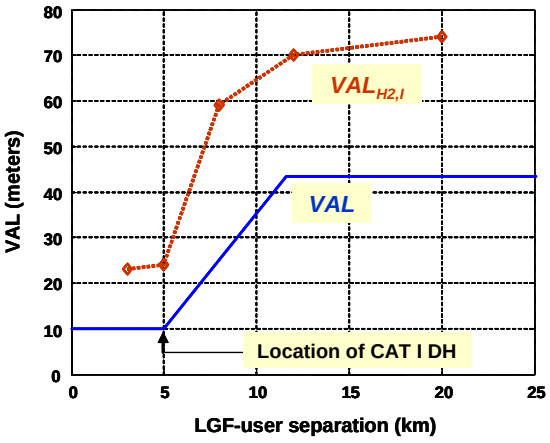

Figure 8. Comparison of "Standard" VAL and Proposed $VAL_{H2,I}$

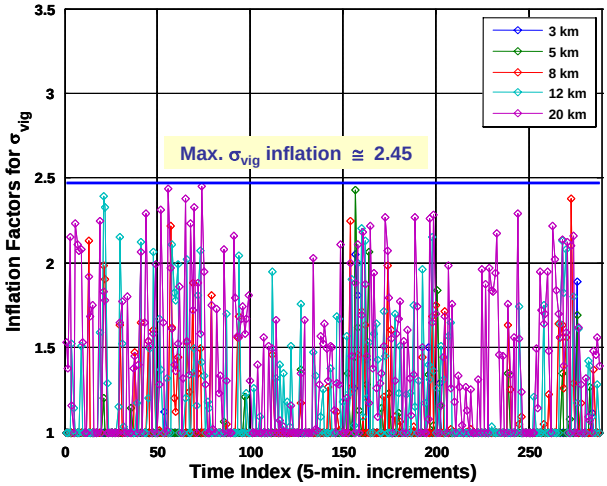

Figure 9. Example Required σ_{vig} Inflation for Memphis LGF

new approaches is incomplete; thus the plotted curve of $VAL_{H2,I}$ as a function of LGF-to-user separation shown in Figure 8 is an example agreed to by both Stanford and the FAA for preliminary use in LAAS ionosphere anomaly analysis. For each time epoch sampled by the position-domain simulation, the simulation must check all subset geometries to see if any usable subset geometries do not satisfy (15). If any such subsets exist, the only degree of freedom left to the GBAS ground station is to increase the broadcast values of σ_{pr_gnd} and $\sigma_{vertical\_ionosphere\_gradient}$ (or σ_{vig}) that contribute to σ_i in (14). Raising VPL_{H0} in this manner makes formerly usable subsets unusable, and all requirements are met when one or both of these sigmas have been raised enough that all usable subsets (with nominal sigma values) that did not satisfy (15) have now become unusable. Note that increasing σ_i in the nominal VPL (14) does not also increase σ_i in the (anomaly-driven) MIEV calculations in (12,13).

A detailed iterative process for finding the inflation factors needed to meet these requirements in real time (the fifth element of Figure 5) is described in [1]. Starting with a fixed value of σ_{pr_gnd} equal to 2.5 times the "GAD-C3" smoothed pseudorange error curve defined in Appendix D of [10] (this amount of inflation was chosen because it exceeds the amount of σ_{pr_gnd} inflation needed to bound nominal errors in the tails of the error distribution, but not dramatically), this algorithm progressively increases the σ_{vig} multiplier in small steps of 0.05 and re-calculates VPL_{H0} for the remaining usable subset geometries that satisfy (15) until they all become unusable (the value of σ_{vig} that bounds nominal errors in CONUS is 4 mm/km – see [13]).

Figure 9 shows the results of this process for an LGF located at the airport at Memphis, Tennessee using the RTCA-standard 24-satellite GPS constellation originally defined in [12]. Note that the amount of σ_{vig} inflation required varies considerably with time and with the particular user-to-LGF separation in a non-monotonic fashion (larger separations usually, but not always, require larger inflation factors). For Category I operations, all separations out to 10 n.mi. (18.5 km) beyond the decision height must be protected, so the required inflation factor in Figure 9 is the maximum among the separations shown for each epoch if the decision height is 3 km or more from the LGF.

Because of the significant variation with time, the most desirable means of determining σ_{vig} inflation factors would be to include the required algorithms inside the GBAS ground station but with a reduced priority relative to the processes that must be

updated at the 2-Hz Type-1-message update rate [6]. This is computationally intensive but is far from impractical because the results of the range-domain simulations (the first and second elements of Figure 5) are performed ahead of time and are pre-stored in a convenient lookup-table format (the third element of Figure 5). However, the approach taken for LAAS is to compute inflation factors for each LGF site ahead of time using an offline simulation. Since real-time information is lost, a fixed inflation factor corresponding to the maximum over one day (e.g., 2.45 for σ_{vig} in the case of Figure 9) must be used at all times. In addition, significant conservatism must be added to the fixed inflation factors to account for satellite constellation changes over time. Paradoxically, constellations with more satellites generally have higher inflation factors because they generate more satellite subsets. As a result, the projected fixed σ_{vig} inflation factor for an LGF at Memphis is about 3.2, assuming that this inflation factor will not be updated for 3 years.

4. Variations for Regions outside CONUS

One difficulty in using the methods described in this paper outside of CONUS is that an ionosphere-anomaly database may be partially or wholly lacking for a given region. It is difficult to confidently extrapolate the CONUS threat model in Section 2.2 to other regions, but some attempt must be made so that users outside CONUS can implement GBAS without having to wait many years to observe very rare ionosphere gradients in their region. Because equations (2 – 10) that form the most detailed definition of the CONUS threat model were fitted directly from CONUS data, the primary author of this paper suggests not using these equations outside CONUS and instead using a modified version of Table 2 as the only bounds on *g*, *v*, and *w*. Specifically, outside of CONUS, the maximum gradient for high-elevation, high-speed fronts would increase from 330 to 400 mm/km, and the maximum gradient in all other rows of Table 2 would increase from 125 or 150 to 250 mm/km. The resulting threat model is much more conservative than the CONUS one and thus provides a great deal of margin against the uncertainties that would exist when installing GBAS in a region lacking ionosphere spatial-gradient anomaly data.

In order to mitigate the impact of the more-conservative threat model proposed above, several possibilities exist for reducing the conservatism in the simulation methodology in Section 3; e.g.:

(1) consider the worst-case single-satellite ionosphere impact rather than the worst-case dual-satellite impact;

(2) consider the prior probability of the worst-case ionosphere anomaly to be low enough that additional nominal errors can be neglected (i.e., set $K_{MD} = 0$ in (12,13));

(3) further increase $VAL_{H2,I}$ based on the proposed WAAS example: add 11 meters to the curve shown in Figure 8.

5. Summary and Future Directions

This paper has described the key elements of the approach to ionosphere anomaly mitigation for GBAS-supported Category I precision approach operations in CONUS. These elements include the formulation and validation of an ionosphere anomaly threat model to the degree possible with the available data, the simulation of anomalous ionosphere impacts on GBAS users based on this threat model so that worst-case user impacts can be ascertained, and the iterative determination of broadcast sigma inflation factors to eliminate subset satellite geometries for which unacceptable ionosphere-induced errors occur.

The brightest aspect of future work in this area is the inclusion of airborne ionosphere gradient monitoring in studies of future GBAS support of Category II/III operations. Preliminary studies suggest that this addition will make GBAS much less sensitive to the bounds and interpretation of the ionosphere threat model. If airborne ionosphere monitoring becomes a standard feature of future GBAS avionics, it should dramatically reduce the need for ionosphere-induced sigma inflation.

Acknowledgements

The assistance, advice, and interest of many people in the Stanford GNSS laboratory and the team of people outside Stanford working on the FAA LAAS Program is appreciated, as is funding support from the FAA LAAS Program Office. The opinions discussed here are those of the authors and do not necessarily represent those of the FAA or other agencies.

References

1. J. Lee, *et al*, "Position Domain Geometry Screening to Maximize LAAS Availability in the Presence of Ionosphere Anomalies," *Proc. of ION GNSS 2006*, Fort Worth, TX., Sept. 26-29, 2006.http://waas.stanford.edu/~wwu/papers/gps/PDF/LeeIONGNSS06.pdf
2. S. Datta-Barua, *et al*, "Using WAAS Ionospheric Data to Estimate LAAS Short Baseline Gradients," *Proc. of the ION 2002 National Technical Meeting*, Anaheim, CA., Jan. 28-30, 2002, pp. 523-530. http://waas.stanford.edu/~wwu/papers/gps/PDF/DattaBaruaIONNTM02.pdf
3. A. Ene, *et al*, "A Comprehensive Ionosphere Storm Data Analysis Method to Support LAAS Threat Model Development," *Proc. of ION 2005 National Technical Meeting*, San Diego, CA., Jan. 15-20, 2005.http://waas.stanford.edu/~wwu/papers/gps/PDF/EneQiuIONNTM05.pdf
4. M. Luo, *et al*, "LAAS Study of Slow-Moving Ionosphere Anomalies and their Potential Impacts", *Proc. of ION GNSS 2005*, Long Beach, CA., Sept. 13-16, 2005. http://waas.stanford.edu/~wwu/ papers/gps/PDF/LuoIONGNSS05.pdf
5. J. Lee, *et al*, "Assessment of Nominal Ionosphere Spatial Decorrelation for LAAS," *Proc. of IEEE/ION PLANS 2006*, Coronado, CA., April 24-27, 2006. http://waas.stanford.edu/~wwu/papers/gps/PDF/LeeIONPLANS06.pdf
6. *Minimum Operational Performance Standards for GPS Local Area Augmentation System Airborne Equipment*. Washington, D.C., RTCA SC-159, WG-4, DO-253A, Nov. 28, 2001. http://www.rtca.org
7. S. Datta-Barua, "Ionospheric Threats to Space-Based Augmentation System Development," *Proceedings of ION GNSS 2004*, Long Beach, CA., Sept. 21-24, 2004. http://waas.stanford.edu/~wwu/papers/gps/PDF/DattaBaruaIONGNSS04.pdf
8. S. Pullen, et al, "Simulation Results and Proposed Sigma Inflation Factors for Memphis PSP," Stanford University, Unpublished Draft, Version 1.5, August 7, 2006.
9. *National Geodetic Survey – CORS: Continuously Operating Reference Stations*. Website: http://www.ngs.noaa.gov/CORS/ .
10. *Minimum Aviation System Performance Standards for Local Area Augmentation System (LAAS)*. Washington, D.C.: RTCA SC-159, WG-4, DO-245A, Dec. 9, 2004. http://www.rtca.org
11. B. Pervan, *et al*, *Algorithm Description Document for the Code–Carrier Divergence Monitor of the Local Area Augmentation System*, Illinois Inst. of Technology, MMAE Dept., Prepared for U.S. Federal Aviation Administration, Washington, DC., Version 4, June 24, 2006. http://mmae.iit.edu/profiles/faculty_pervan.html
12. *Global Positioning System Standard Positioning Service Performance Standard*. Washington, D.C., U.S. Dept. of Defense, Oct. 2001. http://www.navcen.uscg.gov/gps/geninfo/2001SPSPerformanceStandardFINAL.pdf
13. J. Lee, et al, "Assessment of Nominal Ionosphere Spatial Decorrelation for LAAS," *Proc. of IEEE/ION PLANS 2006*, Coronado, CA., April 24-27, 2006. http://waas.stanford.edu/~wwu/papers/gps/PDF/LeeIONPLANS06.pdf